Computational Materials Science 69 (2013) 327–334

Contents lists available at SciVerse ScienceDirect

Computational Materials Science

journal homepage: www.elsevier.com/locate/commatsci

Effect of dilute H on crack tip plasticity in Zr

M. Ruda [a,*], G. Bertolino [b], D. Farkas [c], A. Baruj [b]

[a] CNEA – Centro Atómico Bariloche and Univ. N. del Comahue, Av. Bustillo 9500, 8400 Bariloche, Argentina
[b] CONICET – Centro Atómico Bariloche and Inst. Balseiro – U.N. Cuyo, Av. Bustillo 9500, 8400 Bariloche, Argentina
[c] Department of Materials Science and Engineering, Virginia Tech, Blacksburg, VA 24061, United States

ARTICLE INFO

Article history:
Received 10 August 2012
Received in revised form 12 November 2012
Accepted 27 November 2012
Available online 8 January 2013

Keywords:
Fracture
Twinning
Phase transformation
EAM
Zr
Hydrogen

ABSTRACT

We studied the plasticity mechanisms that occur near a crack tip in hcp Zr with dilute amounts of interstitial H impurities. A quasi-static method was used to simulate crack propagation and the atomic interactions were described by the embedded-atom (EAM) type potentials. We analyzed the influence of H atoms on the deformation mechanisms and phase transformations taking place near the crack tip loaded in Mode I. Crack advance was monitored as a function of the applied stress intensity and it was found to depend on the geometry and orientation of the crack and on the specific position of the H interstitials. As in pure Zr, twinning, dislocations, hcp to fcc and hcp to bcc martensitic transformations near the crack tip are competing deformation mechanisms. Dilute amounts of interstitial H in the crack tip region significantly affect this competition. The results indicate that for most orientations the presence of dilute H interstitials leads to an increase in ductility.

1. Introduction

The present paper is a continuation of a previous work [1] where we performed atomistic studies on the deformation mechanisms of crack propagation under Mode I fracture in single crystalline hcp Zr. For applications, such as zirconium fuel claddings, the material usually develops a preferential texture with the [0001] axis parallel to the radial direction. However, since there is a distribution of grain orientations, in [1] we decided to analyze cracks on different planes and orientations. Our results showed that fracture was ductile and we found evidence that twinning, dislocation emission and phase transformation from hcp to fcc or bcc occurred at the vicinity of the crack tip. The type of deformation mechanism and the size of the plastic region depended strongly upon the geometry and crystallographic orientation of the crack. The purpose of the present work is to analyze the influence of dilute H impurities on these mechanisms.

Considering the assessed Zr–H phase diagram [2] at room temperature and low H concentration, H enters interstitially in the hcp α-Zr matrix producing a solid solution, the solubility limit being very low. The terminal solid solubility (TSS) of H in Zr varies from 0.01 to 10 wt. ppm (0.91–912 atomic ppm) over the 293–473 K temperature range. At higher H concentrations, different hydrides form and precipitate: metastable γ hydride (ZrH), δ hydride ($ZrH_{1.5}$ to $ZrH_{1.66}$), ε hydride ($ZrH_{1.66}$ to ZrH_2). Still another metastable hydride ζ(Zr_2H) has been reported recently [3]. The mechanical properties of and γ hydrides have not been measured so far, although results from some recent first principle calculations [4] of elastic properties of all hydrides indicate that the bulk modulus *B* of the ξ and γ hydrides are slightly higher than that of hcp Zr. The same calculations for the δ and ε hydrides give *B* values which are half the value of pure hcp Zr. (Zr2H: 101 GPa, ZrH: 117 GPa, pure hcp Zr: 97 GPa, $ZrH_{1.66}$: 47 GPa, ZrH_2: 44.38 GPa.). The ratio of the bulk to shear moduli *B*/*G* of a material is related to its brittleness (ductility) when it is below (above) a critical value, around 1.75 [5]. The values of *B*/*G* resulting from these first principles calculations suggest that hydride brittleness follows the order of ζ(Zr_2H) > γ(ZrH) > ε(ZrH_2) > δ($ZrH_{1.5}$), with pure α-Zr placed between the γ and ε hydrides.

Experimentally, δ and ε hydrides are much more brittle than the ductile hcp Zr matrix and have been extensively studied due to the technological consequences of catastrophic fracture on hydrided Zr alloys used in nuclear reactors [6]. The exact mechanism of crack formation and propagation under tension in hydrided Zr has been discussed by Puls [7,8] and Kim [9,10]. Regardless of the fracture mechanism, the presence of δ and ε hydrides is related to observed embrittlement of Zr and its alloys.

Concerning the mechanical properties of Zr containing H in solid solution much less experimental data are available, mainly because of the difficulties to obtain hydride-free samples. Bertolino et al. [11] studied crack propagation in Zircaloy at different H concentrations (10–2000 wt. ppm, 912–182,400 atomic ppm) and

* Corresponding author. Tel.: +54 2944 445278; fax: +54 2944 445190.
E-mail addresses: ruda@cab.cnea.gov.ar (M. Ruda), bertolin@cab.cnea.gov.ar (G. Bertolino), diana@vt.edu (D. Farkas), baruj@cab.cnea.gov.ar (A. Baruj).

0927-0256/$ - see front matter © 2012 Elsevier B.V. All rights reserved.
http://dx.doi.org/10.1016/j.commatsci.2012.11.055

found that for low H concentration the fracture mechanisms observed in the scanning electron microscope (SEM) were ductile by nucleation, growth and coalescence of microcavities, while some brittle regions appeared when H content was increased. These samples were always in the two-phase region so that some hydrides were present even in the more dilute conditions. Recently, Yamanaka et al. [12] measured the elastic modulus, the tensile properties and the microhardness of Zr–H solid solutions. The authors made their measurements on Zr samples containing between 40 and 260 wt. ppm of H, from room temperature to 780 K, again in the two-phase region of the phase diagram. They found that the elastic and shear moduli decreased with increasing hydrogen content. Microhardness was also reduced by hydrogen addition and the tensile properties showed an increase in ductility with hydrogen addition.

Impurity effects on fracture behavior are strongly related to the influence of the impurities on surface energies, and measurements of surface properties on the Zr–H system were performed by Zhang, Li and Norton [13] who studied hydrogen segregation on hcp Zr (0001) and (1010) surfaces by static secondary ion mass spectroscopy, work function, Auger electron spectroscopy and nuclear reaction analysis. They concluded that H has a strong tendency to segregate to these surfaces. This can have an important effect on fracture behavior since it favors the formation of free surfaces, therefore promoting crack growth. However, it is important to also understand the effects of the impurities on the mechanisms of plasticity and this is not easily accessible to experiments.

When considering computer simulations of the solid solution of H in Zr, Yamanaka et al. [12] estimated the electronic structure of the Zr–H solid solution using a molecular orbital calculation. From these results they concluded that the solute hydrogen atom in an interstitial site draws off 4d electrons from the metallic bond onto the Zr–H bond, thus weakening the surrounding metallic bonds. Domain et al. [14] and Domain [15] used the Vienna Ab-initio Simulation Package (VASP) to perform density functional calculations in order to study the interaction of H with free surfaces and stacking faults (SF) in the α-Zr–H solid solution. This is an indirect method to assess mechanical properties. They found that H lowered surface excess energies γ_s but had little influence on the critical cleavage stresses. H segregated at stacking faults (SFs) and at screw dislocation cores. In addition, the presence of H increased the Rice's [16] ductility coefficient $D = \gamma_s/\gamma_{us}$ both at the basal and prismatic planes [14]. The ductility coefficient relates the surface energy to the unstable stacking fault energy γ_{us}, indicating that H in solid solution at the crack tip should favor dislocation emission with respect to crack propagation. In all these simulations Domain [15] described the interfacial H content by the coverage ratio $\Theta = n_{oc}/n_{av}$ with n_{oc} being the number of occupied sites and n_{av} the number of tetrahedral sites available in the defect plane, for the same defect area. Because of the limitations of the supercell size in ab initio calculations, the coverage ratios analyzed were $\Theta = 0$, ¼, ½ and 1. Finally, Udagawa et al. [17] also performed ab initio calculations of γ_s and γ_{us} for pure hcp Zr, Zr–H solid solution ($\Theta = 0.1$, 0.25 and 0.5) and Zr hydride ($\Theta = 1$). They defined Θ as the H/Zrratio, the number of H atoms to the number of Zr atoms in the defect plane, so that their definition of Θ does not coincide with the one used by Domain [15]. We will use Udagawa et al. [17] definition of Θ throughout this work. For the solid solution at $\Theta < 0.5$ they obtained a monotonous decrease by 15–34% and 50–100% in γ_s and γ_{us}, respectively, from those in pure Zr, indicating a competing reduction in both brittleness (by enhancing dislocation mobility) and ductility (caused by a lower surface energy). Therefore, they concluded that it is difficult to assess such hydrogen effects on macroscopic ductile/brittle behavior. Again, because of the size limitations of ab initio calculations, the simulations of the solid solution were actually performed in the two-phase region of the Zr–H diagram. It is interesting to note that in the case of the fcc hydride ($\Theta = 1$) assessment, Udagawa et al. [17] obtained a 25% decrease in γ_s but an increase in the unstable stacking energy γ_{us} of 200–300% compared to pure Zr. This suggests that Zr hydrides have an extremely brittle nature due to the combined effects of a smaller γ_s, implying easy generation of new fracture surface, and a larger γ_{us}, as compared to pure Zr.

In all the ab initio calculations on the Zr–H system available in the literature H concentrations are higher than the solid solution terminal solubility. The embedded atom method (EAM) [18] potentials allow simulations to be performed on a much larger number of atoms and therefore, H concentrations within the solid solution phase are easily attainable.

In the present work we used EAM potentials to simulate the propagation of cracks in very dilute solid solutions of H in Zr, expecting to get more insight on the type of mechanisms involved in the process when no hydrides are present. As it was mentioned before, we already have simulated crack propagation on single crystalline Zr at different crystallographic orientations [1]. In the present work, we reproduced the calculation configurations studied in [1] with the addition of H impurities near the crack tip in order to compare the behavior of the crack propagation in Zr–H solid solution to that of pure Zr. We present the study of crack propagation in various crystallographic orientations and including H interstitials in different positions with respect to the crack tip. In the next section, we will discuss the simulation methods and the sample geometries chosen for our study. We then present and analyze the results for each of the selected crack orientations and finally our general conclusions.

2. Simulation methodology

The interactions between atoms are simulated by semi-empirical potentials of the embedded atom type (EAM) [18] where the total energy of a group of atoms is calculated as a function of their position. In order to depict the behavior of Zr and dilute H we need a set of potentials for each element, plus an interatomic potential for the Zr–H pair. All these functions should be compatible. In order to compare with our previous results [1], we used the Zr potentials developed by Pasianot and Monti [19], the H potentials from Daw and Baskes [18] and for Zr–H the potential developed by us [20]. All potentials were made compatible through a transformation to effective pairs and a normalization of the elec-

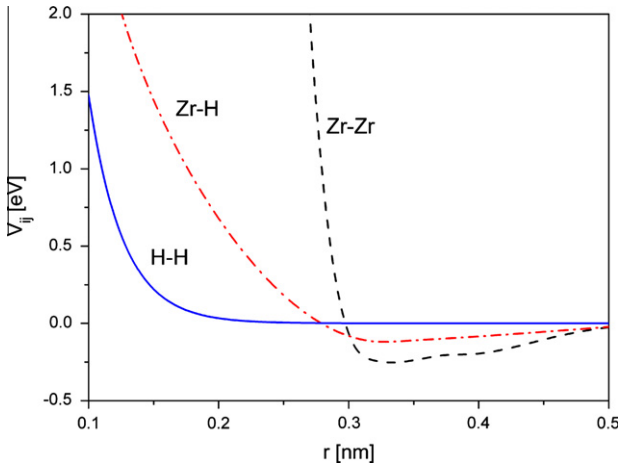

Fig. 1. Pair interactions V_{ij} (eV) for Zr–Zr [19], H–H [18] and Zr–H [20] as a function of the interatomic distance (nm). All potentials correspond to effective pairs (see text).

tronic density as explained in [20]. Fig. 1 shows the pair interactions between all atom types involved.

The Zr EAM potential predicts a stable hcp structure (cohesive energy: $E_{coh} = -6.25$ eV/atom) with respect to fcc ($E_{coh} = -6.23$ eV/atom), bcc ($E_{coh} = -6.14$ eV/atom) and distorted hcp (ω) ($E_{coh} = -6.10$ eV/atom). The potential gives a positive basal I2 stacking fault energy (I2 = 70 mJ/m^2), smaller than the prism stacking fault defect energy (160.8 mJ/m^2). Surface energies for hcp Zr range from 1.070 to 1.437 J/m^2 and surface tension values are1.192 J/m^2 for basal planes, 0.590 J/m^2 for first-order prism planes and 1.211 J/m^2 for second-order prism planes [21].

The Zr–H interaction potential was developed in [20], by fitting to the heat of solution and excess volume of H in Zr. The potential was developed only for dilute concentrations of H in Zr, and it was not intended to be used for hydrides. Concentrations as low as H/Zr = 25 at. ppm (0.27 wt. ppm) can be easily accomplished with the EAM method. A typical first principles calculation may involve less than a thousand atoms or H/Zr = 1000 at. ppm which is a H concentration high enough for hydrides to precipitate. Changes in stacking fault energies and surface properties of Zr due to the presence of H impurities have not been calculated previously with our potential.

In order to study the effect of dilute H in Zr crack propagation we used the same scenario as in Ref. [1] in order to compare to our previous results in pure Zr. We reproduce here the description of the technique to help the reader; further details are available in Ref. [1]. A quasi-static technique has been used to simulate the crack propagation of a semi-infinite crack subjected to an applied Mode I stress intensity factor. Blocks of 40,000 Zr atoms were assembled with dimensions up to 60 nm × 35 nm × 6 nm. An initial atomically sharp crack was inserted with the crack tip at the middle of the simulation block. Periodic boundary conditions were imposed in the direction parallel to the crack front. Displacement boundary conditions were used in the other two directions. The displacements of boundary atoms were fixed at the desired applied Mode I stress intensity factor K_I according to the predictions of the isotropic linear elastic fracture mechanics theory. The interior atoms were then allowed to relax to a minimum energy configuration via a standard conjugate gradient relaxation technique. The applied stress intensity was then increased slowly as to represent equilibrium quasi-static crack growth. The simulations started from a value slightly inferior to the Griffith critical stress intensity factor K_{Ic} and proceeded by small increments of that value. In our conjugate gradient energy minimization procedure we made sure that the forces on every atom were less than 0.01 eV/Å. Further decreasing this convergence criterion did not affect the results.

We chose three different orientations with the crack front running along the $[1\bar{1}00]$, the $[0001]$ and the $[1\bar{2}10]$ hcp directions. Two orthogonal directions were studied for a total of six different sample geometries. Again, this procedure was applied in order to compare with our previous results on pure Zr [1]. Since our goal was to analyze the effect of dilute H on crack propagation and phase transformations in Zr, we introduced the H impurities at different positions near the crack tip. In Fig. 2 we show the H impurities (red on-line) at their initial positions, after relaxation. The average H/Zr atomic concentration is 1:40,000 (0.27 wt. ppm, or 25 at. ppm).

In our results we could analyze the crystalline environment for each atom on the simulation box. The procedure used was the common neighbor analysis (CNA) implemented in the OVITO [22] program. This analysis provides an easy visualization of the mechanisms occurring near the crack tip, such as dislocation emission, twin emission and phase transformations.

To study the relative resistance to crack propagation in the various geometries used we measured the crack advance as a function of the applied Mode I stress intensity factor [1]. Because we used molecular statics energy minimization, the effects of temperature are not included in our simulations. The results are representative of crack propagation resistance at zero temperature. In molecular statics we obtain a minimum energy configuration at each step which is considered to be the equilibrium configuration of the crack tip at the particular loading level [23]. H atoms are free to move to a minimum energy configuration, even though thermal diffusion of H has not been taken into account. We expect most of the trends observed to also hold at finite temperatures, but the lack of thermal effects is an intrinsic limitation of the technique used here. Grain boundary effects on crack propagation will be analyzed in future work.

3. Results

3.1. Effects of H on surface energies and generalized stacking fault energies

Fig. 3 shows a summary of the effects of the interstitial H additions on the surface and generalized stacking fault energies predicted by the Zr–H potential. In all cases studied the presence of H results in a decrease of the surface energy. This decrease is irrespective of the surface orientation, in agreement with previous work as described in the Introduction. These effects would suggest an increased brittle behavior as H is added. The other important parameter that is related to ductile/brittle behavior is the unstable staking fault energy, which can be associated to the ease of dislocation emission and is shown in Fig. 3 center. The effects of H on the values of γ_{us} depend on the plane considered. The parameter D, which is usually considered when studying ductility, has been introduced by Rice [16] as the ratio between γ_s and γ_{us}. This parameter is shown on the right side of Fig. 3 and it suggests decreased ductility as H is added. For the basal plane however, we can see an increase in ductility with increasing H concentration at the more dilute solutions, and the reverse behavior after a certain Θ ratio. These parameters are indicative of averages along the plane of the surface or incipient slip plane, and do not take into account local effects that may vary in the vicinity of the interstitial. These numbers do not take into account twinning as a deformation mechanism and certainly not a stress-induced phase transformation such as was observed in our previous studies of pure Zr [1].

3.2. Stress intensity factor analysis

To study the relative resistance to crack propagation in the selected geometries we measured the crack advance as a function of the applied mode I stress intensity factor K_I. The results for samples of pure Zr and Zr with dilute amounts of H appear in Fig. 4a and b respectively.

What we can see from these curves is that H is an impediment to crack advance, except in one case where the crack front is on the basal plane. We next study with more detail the mechanisms involved in all cases in an attempt to elucidate the role of H in crack propagation.

3.3. Microstructure evolution with crack propagation

On our previous paper [1] we presented the microstructure evolution around the crack tip for pure Zr. To facilitate the reader the comparison with the new results with H impurities we reproduce here the CNA images of the pure Zr next to the results of the equivalent cases with H. In all cases analyzed in this section the configurations presented on graphs correspond to a stress intensity factor $K_I = 1.92$ MPa m$^{0.5}$. Further details about the pure Zr can be obtained from Ref. [1].

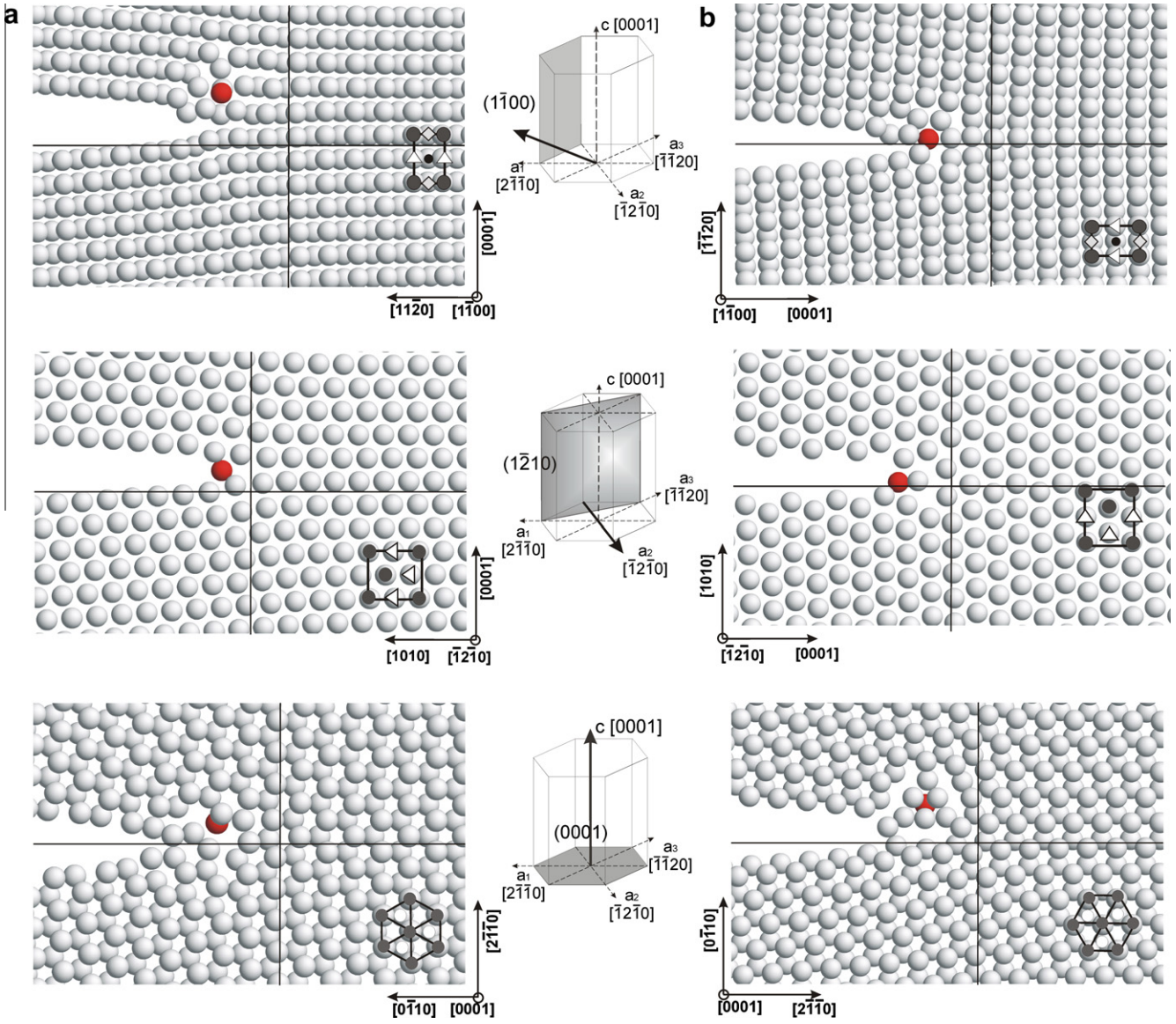

Fig. 2. Geometries analyzed with H impurities (red on-line) at their initial positions, after relaxation. The configurations corresponding to column (a) are orthogonal to those in column (b). (For interpretation of the references to color in this figure legend, the reader is referred to the web version of this article.)

3.3.1. Cracks with a ⟨1 $\bar{1}$ 0 0⟩ crack front

Fig. 5 shows the microstructure of the sample with the crack front along the [1 $\bar{1}$ 00] axis, advancing at the direction [11$\bar{2}$0] after final loading K_I = 1.92 MPa m$^{0.5}$. Both cases for pure Zr and Zr with H initially shown in Fig. 3b are presented. H has arrested the crack propagation, with an advance of 4.03 nm for pure Zr and only 1.74 nm for the case with H at the final loading K_I = 2.96 MPa m$^{0.5}$.

Due to the location of interstitial sites in an hcp lattice, the H atom was originally in a non-symmetrical position and slightly apart from the center of coordinates. After the final loading the vicinity of the crack closer to the H impurity was modified compared to the H-free zone. Because of the vicinity of the H impurity the twinning and the grain formed near the crack tip in pure Zr (Fig. 5a) were replaced by a zone of hcp to bcc phase transformation. Twinning occurred within the bcc phase (Fig. 5b). The presence of the H impurity promoted the transformation to bcc and slowed down the crack propagation.

On Fig. 6 we can see the results of crystal structure at the final loading K_I = 1.92 MPa m$^{0.5}$ for a crack advance along the [0001] direction. For pure Zr, a bcc zone is shown occupying the region of typical plastic deformation near the crack tip. Again, the presence of H stabilizes the bcc phase and the crack advance is restricted, advancing 5.24 nm for pure Zr and 2.10 nm for the case with H at the final loading K_I = 2.96 MPa m$^{0.5}$. The bcc transformed region grows in the direction of the crack tip advance and increases in importance as H are added, resulting in increased blunting of the crack tip.

3.3.2. Cracks with a ⟨1$\bar{2}$10⟩ crack front

On Fig. 7 we can see the final configuration of the crack tip region for the crack advancing along the direction [10$\bar{1}$0] on the ⟨1$\bar{2}$10⟩ crack front. The presence of H promoted and enhanced the dislocation formation around the crack tip; twinnings that were present at the pure Zr configuration disappeared with H. The region of phase transformation to fcc is enhanced. The crack advance is slightly restricted, advancing 2.85 nm for pure Zr and 1.13 nm for the case with H at the final loading K_I = 2.96 MPa m$^{0.5}$. The crack tip is less blunt than in the pure Zr case.

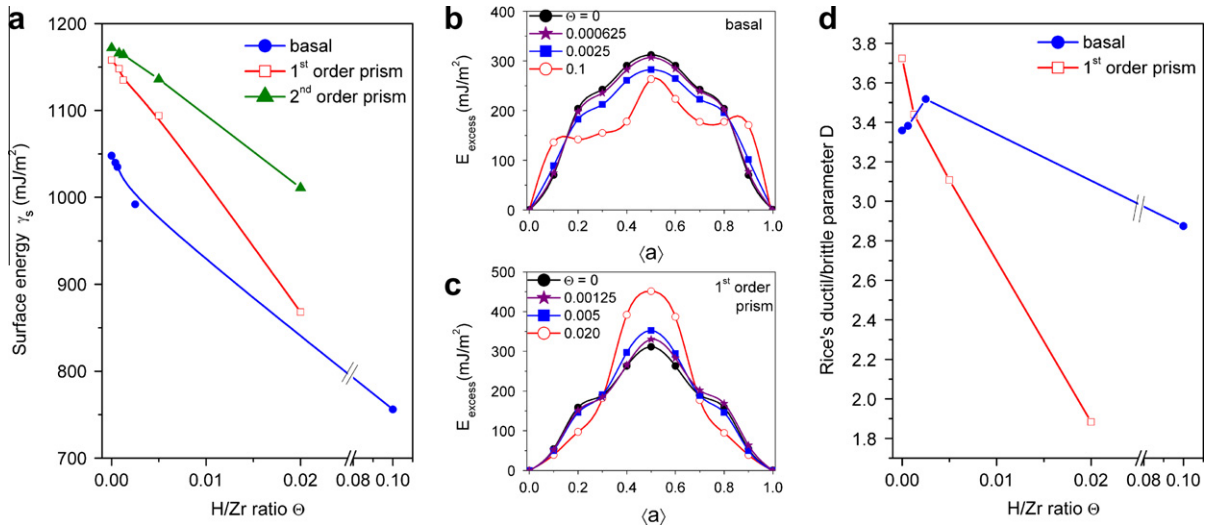

Fig. 3. Variation of the surface and generalized stacking fault energies predicted by the Zr–H potential with H/Zr ratio Θ as defined on text. Left (a): Surface energy (in mJ/m^2) for basal (circles), 1st order prism (squares) and 2nd order prism planes (triangles). Center: (b) Gamma-surface excess energy (in mJ/m^2) profile along ⟨a⟩ in the basal and (c) 1st order prism planes, Θ ratio increases from 0 (filled circles) to larger concentrations (stars, filled squares and empty circles). Right (d): Rice's ductile/brittle parameter D for basal (circles) and 1st order prism planes (squares).

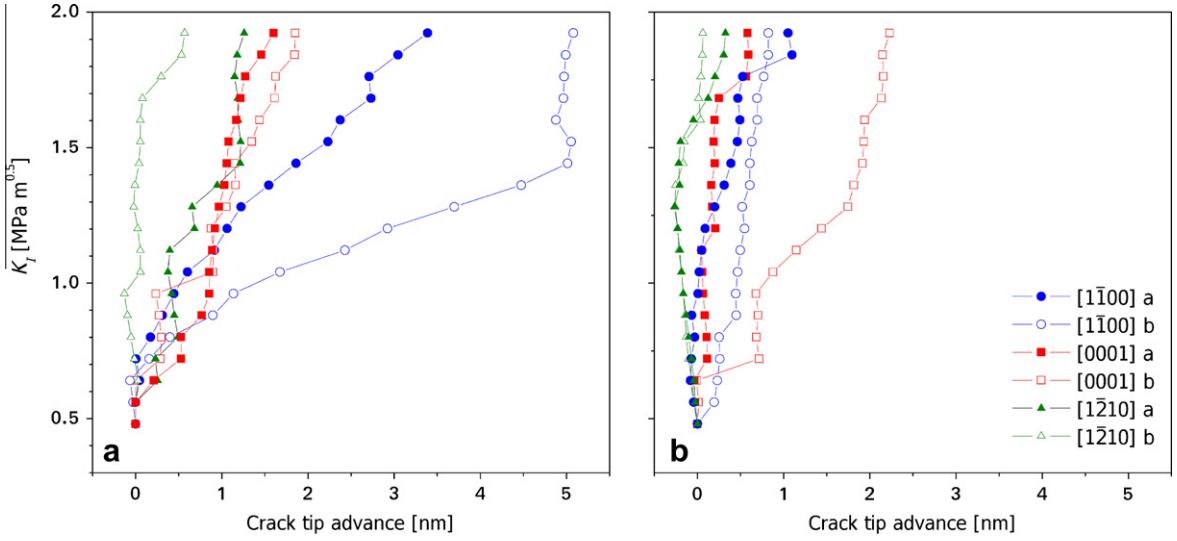

Fig. 4. Stress intensity factor K_I vs crack advance for: (a) pure Zr and (b) H in Zr set initially as shown in Fig. 2. Full symbols correspond to initial configurations shown on the left side (a) of Fig. 2, empty symbols to configurations shown on the right side (b) of that Figure. Triangles (green on line) correspond to crack front on prism planes. Circles (blue on line) correspond to crack front on second type prism planes. Squares (red on line) correspond to crack front on basal planes. (For interpretation of the references to color in this figure legend, the reader is referred to the web version of this article.)

On Fig. 8 the crack propagates along the [0001] direction. The main deformation mechanisms on pure Zr are phase transformations (hcp to fcc and hcp to bcc) and some dislocation activity. When H is present the transformed zones are modified (transformed regions are much smaller), but we can observe more dislocations being formed around the crack tip. The crack advances were similar (2.07 nm for pure Zr and 0.73 nm for the case with H at the final loading $K_I = 2.96$ MPa m$^{0.5}$). In both cases where H enhanced the amount of dislocations we can observe that the crack tip is less blunt that for pure Zr.

3.3.3. Cracks with a ⟨0001⟩ crack front

For cracks with a ⟨0001⟩ crack front in pure Zr the main deformation mechanisms that took place near the crack tip were: transformation to bcc, twinning within the transformed bcc phase and dislocations emission [1]. On Fig. 9 we can see the results for the crack advancing on the [2$\bar{1}\bar{1}$0] direction with and without H. The regions of phase transformations are much smaller for the case with H, and the crack advance was restrained compared to the pure Zr case, advancing 2.53 nm for pure Zr and only 0.32 nm for the case with H at the final loading of $K_I = 2.96$ MPa m$^{0.5}$.

When we considered the same geometry as before but with the crack in a position orthogonal to the one just analyzed ([0$\bar{1}$10] direction) and H situated initially as shown in Fig. 2 we found H to help the propagation of the crack. We decided to study this case with more detail and placed the H impurity in different sites. The initial positions of H after relaxation are shown on inserts on Fig. 10. On Fig. 10b H was placed on the same position as on Fig. 2b. On Fig. 10c and d H was initially (after relaxation) on the line of the horizontal axis, 0.3 nm and 3 nm apart from the crack tip respectively. On the same figure we depicted the results after applying a stress intensity factor of $K_I = 1.92$ MPa m$^{0.5}$. We can

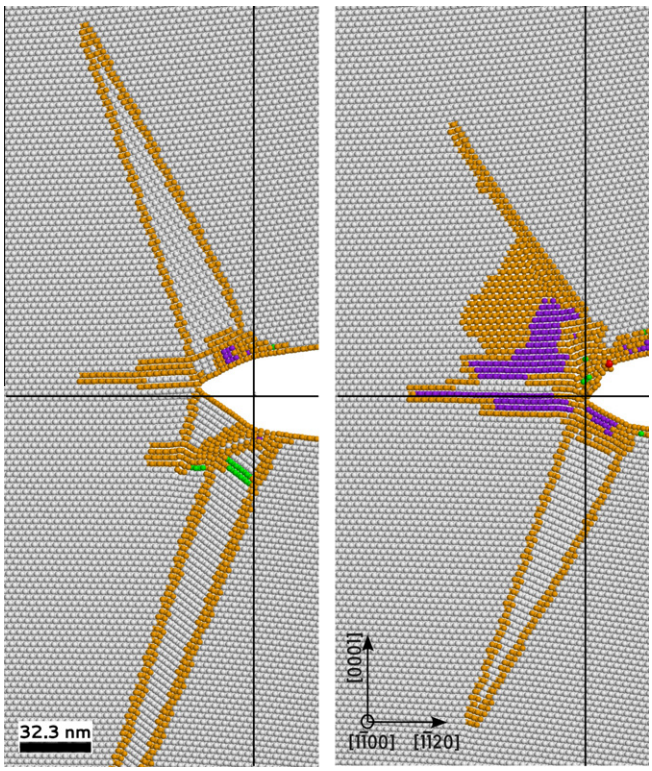

Fig. 5. Crack front along the [1 $\bar{1}$ 0 0] axis advancing at the direction [1 1 $\bar{2}$ 0] after loading K_I = 1.92 MPa m$^{0.5}$. (a) Pure Zr and (b) with H impurity as shown in Fig. 2 for initial conditions after relaxation. CNA shades of grey (on-line colors) for atoms in different structures are: hcp: white (white); fcc: light grey (green); undefined: grey (gold); bcc: dark grey (purple); bcc twins: black (black). H impurity is red on-line. (For interpretation of the references to color in this figure legend, the reader is referred to the web version of this article.)

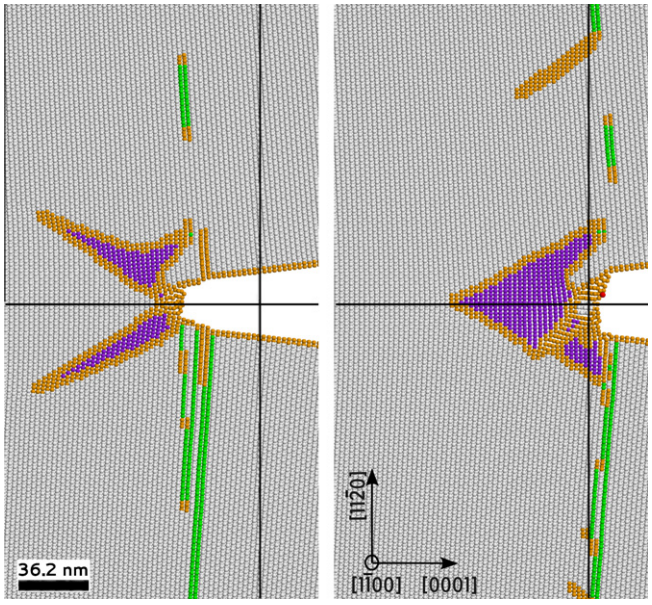

Fig. 6. Crack front along the [1 $\bar{1}$ 0 0] axis, direction [0 0 0 1] after loading K_I = 1.92 - MPa m$^{0.5}$. (a) Pure Zr and (b) with H impurity as shown in Fig. 2 for initial conditions after relaxation. CNA shades of grey (on-line colors) for atoms in different structures are: hcp: white (white); fcc: light grey (green); undefined: grey (gold); bcc: dark grey (purple); bcc twins: black (black). H impurity is red on-line. (For interpretation of the references to color in this figure legend, the reader is referred to the web version of this article.)

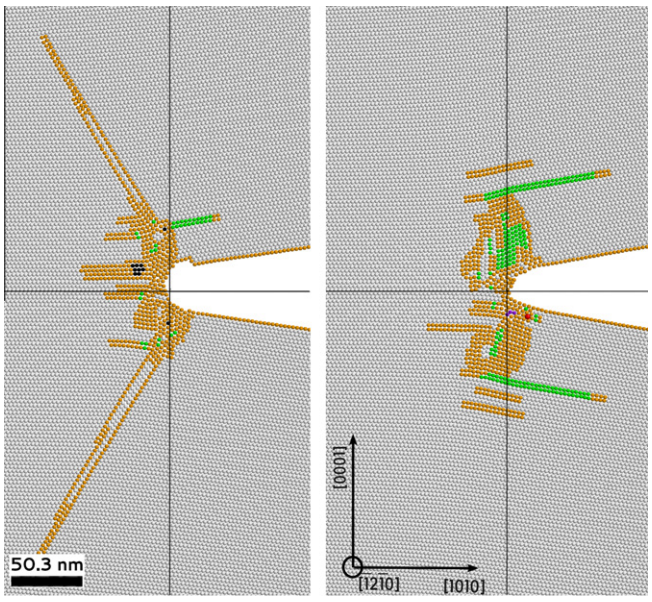

Fig. 7. Crack tip configuration of the crack front along [$\bar{1}$ 2 $\bar{1}$ 0] axis, direction [1 0 $\bar{1}$ 0] after K_I = 1.92 MPa m$^{0.5}$. (a) Pure Zr and (b) with H impurity as shown in Fig. 2 for initial conditions. Common neighbor analysis shades of grey (on-line colors) for atoms in different structures are: hcp: white (white); fcc: light grey (green); undefined: grey (gold); bcc: dark grey (purple); bcc twins: black (black). H impurity is red on-line. (For interpretation of the references to color in this figure legend, the reader is referred to the web version of this article.)

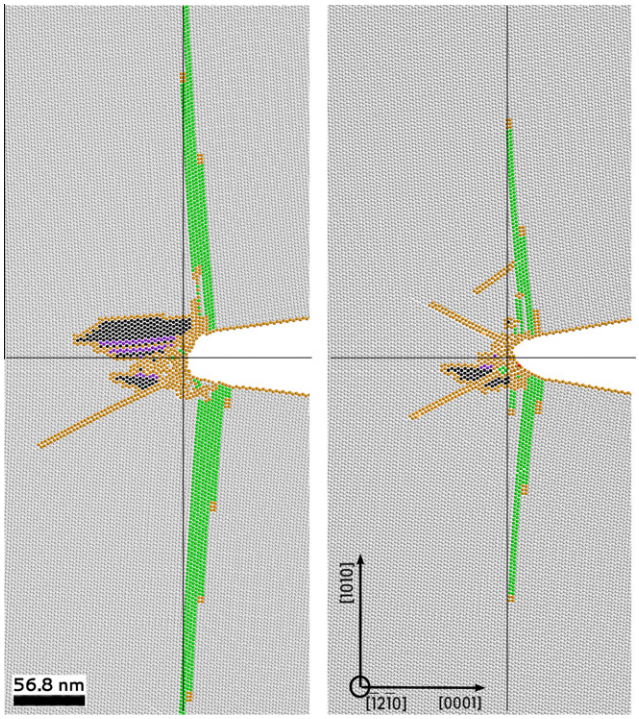

Fig. 8. Crack tip advance of the crack front along [$\bar{1}$ 2 $\bar{1}$ 0] axis, direction [0 0 0 1] after K_I = 1.92 MPa m$^{0.5}$. (a) Pure Zr and (b) with H as shown in Fig. 2 for initial conditions. Common neighbor analysis shades of grey (on-line colors) for atoms in different structures are: hcp: white (white); fcc: light grey (green); undefined: grey (gold); bcc: dark grey (purple); bcc twins: black (black). H impurity is red on-line. (For interpretation of the references to color in this figure legend, the reader is referred to the web version of this article.)

observe that, when H was on the line of the horizontal axis of the crack (cases (c) and (d)) the regions where phase transformations took place were modified and the crack advance was arrested. This

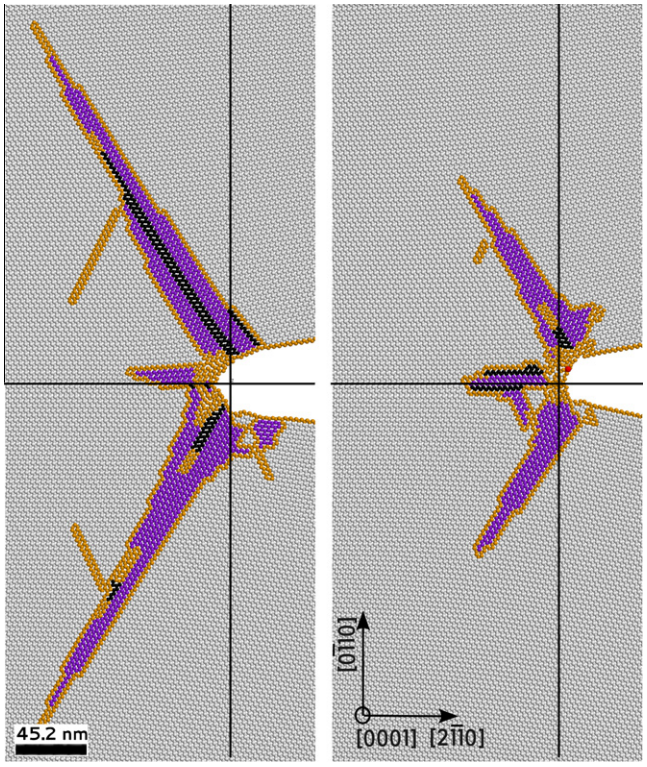

Fig. 9. Crack tip advance of cracks with crack fronts along the [0001] axis, direction [2$\bar{1}\bar{1}$0] after K_I = 1.92 MPa m$^{0.5}$. (a) Pure Zr and (b) with H as shown in Fig. 2 for initial conditions. Common neighbor analysis shades of grey (on-line colors) for atoms in different structures are: hcp: white (white); fcc: light grey (green); undefined: grey (gold); bcc: dark grey (purple); bcc twins: black (black). H impurity is red on-line. (For interpretation of the references to color in this figure legend, the reader is referred to the web version of this article.)

is confirmed by the curves shown in Fig. 11. When the H impurity was 3 nm away from the crack tip, the initial distortion of the lattice influenced the transformations occurring between the position of the H and the crack tip. However, when H was initially slightly displaced from the crack line, it ended up adsorbed on one the fracture surfaces and the crack could proceed more easily than in the case of pure Zr.

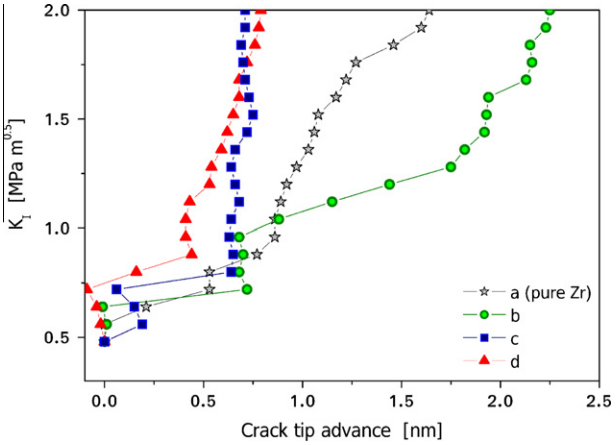

Fig. 11. Stress intensity factor K_I vs. crack advance for: pure Zr and H in Zr set initially in different sites as shown in Fig. 10.

4. Discussion

An analysis of the various cases examined shows that crack propagation in Zr is strongly affected by the crystal orientation and the presence of H at low concentrations. Fig. 4a shows a summary of the crack advance behavior for all cases studied in pure Zr, whereas Fig. 4b shows the same data for the materials containing dilute H impurities in the crack tip region. This comparison clearly shows that in the great majority of cases, crack advance is retarded by the presence of the dilute H. There are significant differences in the behavior of cracks with different crystallographic orientations, even in the absence of impurities. Consider for example the case of the crack front parallel to the normal of the first type prismatic plane and advancing in the [0001] direction. For an applied K_I = 1.92 MPa m$^{0.5}$, the crack advanced about 10 times more than a crack with the same growth direction [0001], but with the crack front normal to a prismatic plane of the second type. The differences are even larger at a lower stress intensity value. The origin

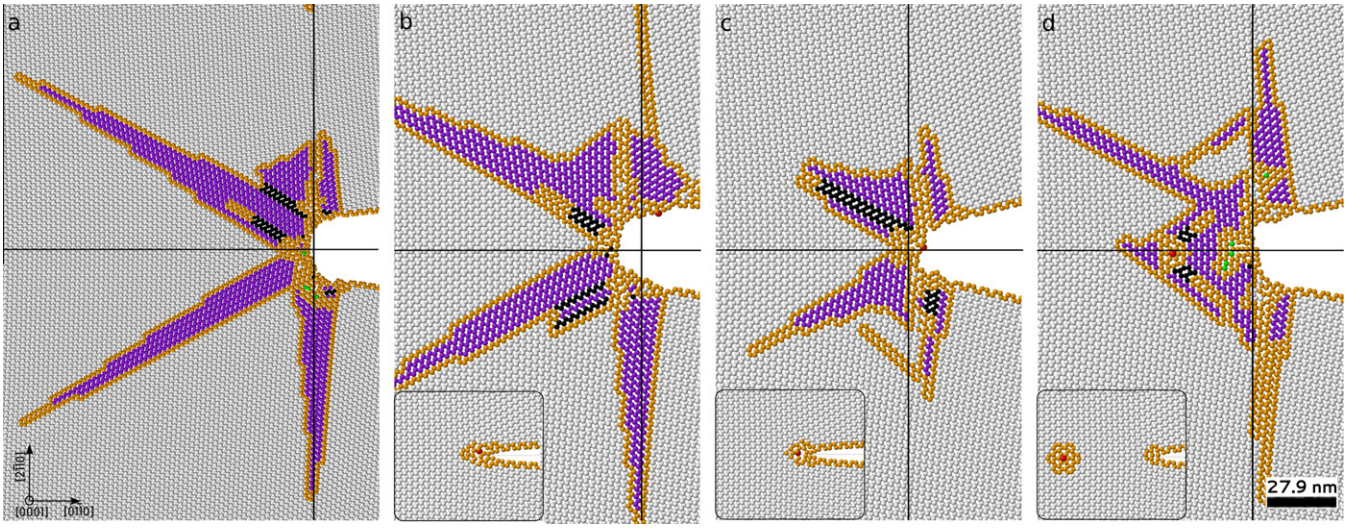

Fig. 10. Crack tip advance of cracks with crack fronts along the [0001] axis, direction [0$\bar{1}$10] after K_I = 1.92 MPa m$^{0.5}$. (a) Pure Zr and (b–d) with H initially as shown on inserts (after relaxations). Common neighbor analysis shades of grey (on-line colors) for atoms in different structures are: hcp: white (white); fcc: light grey (green); undefined: grey (gold); bcc: dark grey (purple); bcc twins: black (black). H impurity is red on-line. (For interpretation of the references to color in this figure legend, the reader is referred to the web version of this article.)

of the differences resides exclusively in the crystal orientation and the particular mode of deformation which takes place in each case. In the cases where the crack advances more at the same stress intensity factor the formation of relatively bounded areas of transformation to bcc can be seen (Fig. 6a). The cases showing less crack propagation are associated with fcc transformation and generation of a larger deformed area ahead of the crack tip (Fig. 7a). The explanation then is that the fcc transformation is relatively simple for an hcp material, it occurs by the introduction of stacking faults every two planes. In comparison, the bcc transformation is more complex because, among other factors, it implies significant volume change. Given a suitable orientation, the phase transformations mechanisms are activated and absorb much of the mechanical energy applied, thus reducing the energy available to break interatomic bonds and to form the new surfaces associated with the fracture process. Twin generation and dislocation emission are also competing mechanisms occurring near the crack tip. Their effect is less important in terms of energy than that of the phase transformations near the tip region [1].

The addition of a small concentration of H in the vicinity of the crack tip alters the process of crack propagation. In all cases studied but one, the presence of H retards crack advance (Fig. 4b) and modifies the patterns of the associated plastic zones compared to the analogous situation without H. The presence of H in the tip region is associated with a distortion of the lattice, even without applied load (see Fig. 2). With the application of load, this distortion leads to a rounding effect on the crack tip, which in general should reduce the stress concentration in this zone. However, one should expect that if the crack advances beyond the H position, the volume distortion associated with H should act in the opposite direction, i.e. facilitating the generation of new surfaces and locally accelerating the advance of the crack front. This is the case observed in the results obtained for H near the crack tip in the basal plane at the [0 0 0 1] direction. When the H atom remains in the line of the crack front, the crack tip is rounded (Fig. 10c and d) and the crack advance is delayed. If the H atom is initially located slightly above the crack line it ends up adsorbed on one of the lips of the crack (Fig. 10b) and the crack proceeds to a larger extent than without H (Fig. 10a). In most cases we observe that the effects of the H impurities depend on the specific position of the interstitial with respect to the crack tip.

Besides the phase transformations, other plasticity mechanisms that are changed by the presence of H are twinning and dislocation emission near the crack tip. We observe less amount of twinning (Figs. 5 and 7) and an enhancement of dislocation emission (see Fig. 6) with the presence of H. Again, the extent of these effects is critically dependent on the crack orientation and the exact position of the interstitial H.

These results show that the texture of the material is critical to control the advance of cracks. They also explain the experimental observations made by other researchers that indicate an increase in ductility at low concentrations of H in Zr [4,11,12].

In the particular situation of the Zr–H system, H has a relatively large atomic volume compared to the volume of the interstices of the hcp lattice, so that the H impurity causes a local distortion of the Zr matrix (Fig. 2). The presence of a crack under load involves the generation of a high stress region ahead of the crack tip. When the H atoms are present in the crack tip area, they find favorable conditions for accommodating themselves in interstitial sites near the front of the crack. In particular, due to the stress concentration at the crack tip, the sites located along the axis of advance of the crack are more favorable because they have the largest available volume. This reasoning can constitute a possible explanation for the effect seen in the simulations presented here, since this mechanism interferes with the advance of the crack resulting in an increase in ductility that may be seen macroscopically.

Finally, we note that increased ductility resulting from dilute H interstitials can not be explained by applying the Rice criterion only. We showed examples where the Rice ductile/brittle parameter decreased with the addition of H, suggesting a decrease in ductility; yet the crack advance was arrested. The reason for this behavior is the complex interplay and competition among the various plasticity mechanisms and elastic effects that are influenced by the presence of dilute H.

5. Conclusions

Our atomistic simulations show that twinning, dislocation emission and phase transformations occur near the crack tip region during low temperature fracture of hcp Zr with and without H impurities. The relative importance of these plasticity mechanisms depends on the crystallographic orientation of the crack.

A dilute amount of H impurities placed at different distances from the crack tip significantly affects the competition between crack propagation, twin generation, dislocation emission and phase transformations in the crack tip region. Dilute interstitial H in the vicinity of the crack tip also modifies the size of the phase transformation regions observed and in most cases, leads to an increase in ductility in single crystalline Zr.

Acknowledgements

This work was partially supported by Agencia Nacional de Promoción Científica y Tecnológica de Argentina, PAE 36985; Universidad Nacional de Cuyo, Project 06/C399; CONICET/PIP 2011-00056 and the National Science Foundation IRD program.

References

[1] M. Ruda, D. Farkas, G. Bertolino, Comput. Mater. Sci. 49 (2010) 743–750.
[2] E. Zuzek, J.P. Abriata, A. San-Martin, H–Zr (Hydrogen-Zirconium), in: F.D. Manchester (Ed.), Phase Diagrams of Binary Hydrogen Alloys, ASM Int., Materials Park (OH), 2000.
[3] Z. Zhao, J.P. Morniroli, A. Legris, A. Ambard, Y. Kihn, L. Legras, M. Blat-Yrieix, J. Microsc. 232 (2008) 410–421.
[4] W. Zhu, R. Wang, G. Shu, P. Wu, H. Xiao, J. Phys. Chem. C 114 (2010) 22361–22368.
[5] S.E. Pugh, Phil. Mag. 45 (1954) 823–843.
[6] S.-Q. Shi, M.P. Puls, J. Nucl. Mater. 218 (1994) 30–36.
[7] M.P. Puls, J. Nucl. Mater. 393 (2009) 350–367.
[8] M.P. Puls, Comments on author's reply to Review of the thermodynamic basis for models of delayed hydride cracking rate in zirconium alloys, M.P. Puls in J. Nucl. Mater. 393 (2009) 350–367. J. Nucl. Mater. 399 (2010) 248–258.
[9] Y.S. Kim, M.P. Puls in J. Nucl. Mater. 393 (2009) 350–367. M.P. Puls in J. Nucl. Mater. 399 (2010), 240–247.
[10] Y.S. Kim, M.P. Puls in J. Nucl. Mater. 393 (2009) 350–367. J. Nucl. Mater. 399 (2010) 259–265.
[11] G. Bertolino, G. Meyer, J. Perez Ipiña, J. Nucl. Mater. 320 (2003) 272–279.
[12] S. Yamanaka, D. Setoyama, H. Muta, M. Uno, M. Kuroda, K. Takeda, T. Matsuda, J. Alloys Compd. 372 (2004) 129–135.
[13] C.-S. Zhang, B. Li, P.R. Norton, J. Alloys. Compd. 231 (1995) 354–363.
[14] C. Domain, R. Besson, A. Legris, Acta Mater. 52 (2004) 1495–1502.
[15] C. Domain, J. Nucl. Mater. 351 (2006) 1–19.
[16] J.R. Rice, J. Mech. Phys. Solids 40 (1992) 239–271.
[17] Y. Udagawa, M. Yamaguchi, H. Abe, N. Sekimura, T. Fuketa, Acta Mater. 58 (2010) 3927–3938.
[18] M.S. Daw, M.I. Baskes, Phys. Rev. B 29 (1984) 6443–6453.
[19] R.C. Pasianot, A.M. Monti, J. Nucl. Mater. 264 (1999) 198–205.
[20] M. Ruda, D. Farkas, J. Abriata, Phys. Rev. B 54 (1996) 9765–9774.
[21] M.I. Pascuet, R.C. Pasianot, A.M. Monti, J. Mol. Catal. A: Chem. 167 (2001) 165–170.
[22] A. Stukowski, Mater. Sci. Eng. 18 (2010) 015012. See also <http://www.ovito.or>.
[23] D. Farkas, M. Willemann, B. Hyde, Phys. Rev. Lett. 94 (2005) 165502.